Int J CARS (2014) 9:875–889
DOI 10.1007/s11548-013-0975-7

ORIGINAL ARTICLE

4D-CT Lung registration using anatomy-based multi-level multi-resolution optical flow analysis and thin-plate splines

Yugang Min · John Neylon · Amish Shah · Sanford Meeks · Percy Lee · Patrick Kupelian · Anand P. Santhanam

Received: 19 August 2013 / Accepted: 30 December 2013 / Published online: 14 January 2014

Abstract
Purpose The accuracy of 4D-CT registration is limited by inconsistent Hounsfield unit (HU) values in the 4D-CT data from one respiratory phase to another and lower image contrast for lung substructures. This paper presents an optical flow and thin-plate spline (TPS)-based 4D-CT registration method to account for these limitations.
Methods The use of unified HU values on multiple anatomy levels (e.g., the lung contour, blood vessels, and parenchyma) accounts for registration errors by inconsistent landmark HU value. While 3D multi-resolution optical flow analysis registers each anatomical level, TPS is employed for propagating the results from one anatomical level to another ultimately leading to the 4D-CT registration. 4D-CT registration was validated using target registration error (TRE), inverse consistency error (ICE) metrics, and a statistical image comparison using Gamma criteria of 1 % intensity difference in 2 mm^3 window range.
Results Validation results showed that the proposed method was able to register CT lung datasets with TRE and ICE values <3 mm. In addition, the average number of voxel that failed the Gamma criteria was <3 %, which supports the clinical applicability of the propose registration mechanism.
Conclusion The proposed 4D-CT registration computes the volumetric lung deformations within clinically viable accuracy.

Y. Min (✉) · J. Neylon · P. Lee · P. Kupelian · A. P. Santhanam
Department of Radiation Oncology,
University of California, Los Angeles, CA, USA
e-mail: ymin@mednet.ucla.edu

A. Shah · S. Meeks
Department of Radiation Oncology,
MD Anderson Cancer Center, Orlando, FL, USA

Keywords Lung registration · Radiotherapy · Optical flow

Introduction

Recent advances in radiation delivery methods have led to an increased effectiveness in treating lung cancer. However, a key challenge that remains for lung cancer radiotherapy treatment is the ability to know and track the movement of the lung tumor throughout the respiration cycle during the radiotherapy procedure. Undetected and uncompensated lung tumor motion caused by variations in the subject breathing pattern can lead to dose delivery errors and suboptimal radiotherapy. Strategies to adjust for some of these anatomical or positional variations include the use of margins to expand the volume of measured or suspected tumor and the subsequent irradiation of this larger volume (termed the Planning Target Volume, PTV). While the usage of large PTV margins for a lung tumor may lead to overdosage of the normal lung tissues, breathing variations may lead to an under dosage of the lung tumor. The radiation treatment efficacy needs to be further investigated for the radiation dose delivered to a dynamically deforming lung anatomy [1–6].

The class of biomechanical models that reflect the dynamic deforming lung anatomy based on a specific stimulus (e.g., tidal volume change, movement of diaphragm) is referred as physics-based models [7]. The models may include physics-based properties such as Young's modulus and bulk modulus. The usage of such physics-based models leads to adaptive radiotherapy frameworks where the radiotherapy accounts for the organ motion that occurs during the treatment fraction. Recent advances in the field of real-time physics-based deformation models have led to the development of a subject-specific physics-based lung deformation model that can be used for simulating and visualizing the lung tumor motion and the lung surface motion [8]. Physics-based volumetric

lung models that are developed from 4D-CT lung datasets show the lung anatomy (e.g., blood vessels, airways) deformation at different breathing patterns and facilitate accounting for the radiation delivery to both the normal tissues and the tumor.

Physics-based models rely on volumetric displacement values extracted for 4D imaging. To compute the volumetric displacement in physics-based models, registration techniques using the 4D lung anatomy can be used [9,10]. From the volumetric displacements, the full range of tumor location and motion during the respiration cycle can be estimated [11]. However, undetected and uncompensated errors in registration may lead to errors in the physics-based models that may be carried into the adaptive radiotherapy workflow [6]. Registration errors are caused by two limitations: (a) variations in the image voxel HU from one respiratory phase to another and (b) low image contrast in regions such as the parenchyma. Developing a 4D-CT image-based registration algorithm that accounts for these limitations forms the key contribution of this paper.

In this paper, we propose a multi-resolution optical flow and TPS-based 4D-CT lung registration method. To minimize registration errors caused by inconsistencies in the voxel intensity from one breathing phase to another, we used anatomy levels to represent different lung substructures. Each 3D lung volume was segmented into multiple anatomical levels, assigned unified consistent voxel intensity for each anatomy level and registered using the optical flow method at multiple resolutions for each anatomical level separately. The registration results of an anatomical level were then interpolated for the next anatomy level using TPS and used as initial displacement for its multi-resolution optical flow registration. For comparison purposes, results shown in this paper compared the 4D-CT lung images acquired for non-small-cell lung cancer subjects undergoing radiotherapy, estimated the 3D lung displacement from one breathing phase to another using the proposed method, and compared the motion estimation with three different registration methods (multi-resolution optical flow method, free-form registration, and inverse consistent demons method) with a single level of anatomy that includes all the sub-anatomical structures.

Related works

In this section, we further discuss the registration methods used for medical imaging related to our proposed method and registration method validation.

Lung registration methods

Lung registration methods have been extensively investigated in the field of medical imaging as well as in the field of radiation oncology [9,10,12,13] and benchmarked for different input datasets [14]. While a large body of related works exists, a concise review of the 4D-CT lung registration methods is discussed in this subsection. Registration methods can be broadly classified into either parametric or physics-based methods. Parametric methods employ image intensity and additional smoothing-based constraints for registering source images with the target images. Betke et al. [15] presented an iterative rigid body transformation-based approach for registering the lung surface models. This method does not, however, take into account the local continuity in displacement. Additionally, only the surface of the lung was registered. In [14], a B-spline-based registration was discussed with emphasis on its validation. In this registration, the distribution of the landmarks inside the lungs is divided into four sub-anatomical regions for each lung for improving the registration accuracy. A multi-resolution dataset for each lung is created, and a clinical expert tracks the landmark motion on each resolution. The rest of the lung is registered using B-splines. A key issue in achieving intensity-based estimation of the 4D volumetric lung motion is that it is limited by low resolution and low contrast constraints imposed by the 4D-CT data. The low resolution and contrast of the 4D-CT data are a result of the steps taken to minimize the radiation exposure to the subject from 4D-CT imaging. In a free breathing image, the low spatial contrast in the voxel intensity combined with the image noise renders the key landmarks to have different HU values at different air volumes inside the lung. Yin et al. [16] discuss an approach to address the intensity variation using a B-spline-based approach coupled with a cost function that characterizes the HU values of voxels as a combination of tissue and air and minimizes the differences in the squared tissue volume.

Physics-based registration methods are mainly used in conjunction with parametric methods to include additional constraints. This yields a cost function, which can subsequently be minimized to obtain the registration. In an early work [17,18], a method where a few landmarks, namely the airway bifurcations, were tracked from one volume to another is presented. The surrounding anatomy was registered from one volume to another using a continuum mechanics approach. Three main constraints used are non-compressibility, divergent free, and continuity preserving. Similar efforts by peers [19–21] propose forward and inverse based estimation of the lung image registration. The forward step is where the source is registered to the target and then inversely the target is reregistered to the source. This is used to define a cost function that minimizes the difference between the forward and the inverse registration. The forward and inverse transformations themselves are taken as vectored values, and their difference is minimized. Ding et al. [22] used this lung registration-based assessment for estimating the lung tissue mechanics. Specifically, the lung

datasets are registered using an inverse consistent approach. The Jacobian value is then computed for each voxel position. When the Jacobian is positive, the tissue at that voxel is considered to be expanding; otherwise, it is contracting. Furthermore, Pan et al. [23] completed a lung registration-based assessment of the local lung tissue expansion. The registration was done using inverse consistent image registration and validated using xenon CT imaging. As a comparison parameter, the Jacobian value for each voxel is measured and compared with the xenon CT imaging. The work presented a manual way to register landmarks from one airway branching tree to another. It is followed by a cost minimization function that when minimized will give the registration of all the other points. The cost minimization includes linear elasticity constraints and the reverse displacement constraints. The method, however, assumes constant and linear elastic parameters, which may not be accurate for every subject.

Optical flow methods

Optical flow-based registration has been widely investigated in different domains of image-based motion tracking [11]. The optical flow registration method tracks the 2D/3D motion of 3D objects using multiple images of the objects in motion. The method characterizes a 3D object in 2D images as features and correlates the features from one image to another in such a way that the cumulative intensity displacement gradient is minimized. For clarity, the method is briefly discussed.

The optical flow registration method starts with an initial estimated displacement (typically set to 0 for each voxel) and then refines it according to partial derivative of voxel intensity and weighted sum of displacement from all nearby voxels. Displacement estimation is iteratively updated until the displacement in the whole field converges [24]. The advantage of this method is that it manages to track the overall motion of the field even if some feature points cannot be tracked.

The optical flow registration method, however, has some limitations in 4D-CT lung data registration, which reduces the overall accuracy of the lung registration. First, the optical flow algorithm assumes small displacement, since the first partial derivative of intensity relies on Taylor series expansion, which is only valid with small changes. The accuracy is decreased if the displacement is larger than 1 voxel distance. Zhang et al. [11] use a multiple resolution algorithm to address the issue. This method is based on the fact that a large voxel distance between any two voxels in an image becomes smaller when the resolution of the images is reduced. The method works as follows. For any given pair of source and target images, the displacements of each feature in the source are first calculated using the lowest resolution of both the source and the target images. The initial value of the displacement at this resolution is considered to be 0. The computed displacement at the lowest resolution is propagated to the image pair at the next resolution as the initial value of displacement. This process is repeated for the image pairs at each resolution until the displacement is computed for the highest resolution image pair.

The accuracy of the multi-resolution optical flow is limited by the fact that the displacement accuracy of one voxel depends on the accuracy of nearby voxels and is affected by the non-constant intensity of the landmarks in the image data. From the CT imaging perspective, the HU value represents the photon attenuation of an anatomical location. Due to the lung motion and large air volume change inside the lung during respiration, the photon attenuation of the same point may change from one respiratory phase to another. Studies in our institution have shown that the HU values of the 3D lung anatomical structures do not remain constant for the entire 4D image dataset. This observation is further detailed in "Landmark intensity variation studies" section. Nevertheless, such registration error is introduced into both the single and multi-resolution optical flow because of the constant intensity assumption and needs to be further investigated and addressed.

Additionally, in the case of lungs, the volume is composed of different anatomical components that each requires a different weight during registration. Each anatomical constituent (e.g., blood vessels, airways) is known to have a different HU value. The method proposed in the paper performs optical flow-based registration at each level of anatomy separately thereby preventing the propagation of errors from anatomical level to another.

Anatomy level-based registration

The usage of multiple anatomical levels for the lung registration is analogous to the creation of anatomical maps for brain image registration using posterior probabilities distribution and Kullback Liebler divergence [25]. However, the usage of hierarchical anatomical maps for lung 4D-CT registration is a novel contribution of the proposed work. The HAMMER algorithm has been proposed as a hierarchical approach for brain image registration [26,27] and uses the forward and backward propagation matching for registering the sparse set of landmarks for three anatomical levels inside the brain. The rest of the pixels are registered using a TPS algorithm. Wu et al. [28] used a similar hierarchical approach for registering a free breathing CT with 4D-CT lungs. Landmarks in the blood vessels were acquired using a seed-growth-based segmentation algorithm and registered using a single resolution $L2$ norm cost function minimization. The cost function did not include the intensity values directly but included the local morphology. Once the landmarks were registered, the rest of the lungs were registered using TPS algorithm.

Validation of registration methods

Validation of 4D-CT registration methods is pivotal in quantitatively representing the accuracy in representing the volumetric lung motion. Quantitative measures such as TRE, Gross Tumor Volume, Jacobian value, and inverse consistency error have been used for validating registration algorithms. The number of datasets used in each of the validation procedure varied from 1 end-inspiration end-expiration pair to 13 4D-CT datasets. A seminal comparison study is presented by Vik et al. [29] to give some validation perspective between four different classes of registration methods, point-based tracking, surface-based tracking, parametric volume-based registration, and nonparametric volume-based registration using 10 end-expiration and end-inspiration CT datasets. From the focus of radiation oncology, the study showed that the surface-based registration is slightly more accurate than the other registration methods. From a validation perspective, it was shown that the TRE-based estimation of the dose validation and inverse consistency together was a satisfactory measure for representing the registration accuracy. Additionally, Murphy et al. [14] discuss the accuracy of the landmarks with the mean inter-observer difference shown to be at least 2 ± 1 mm. Variations in the accuracy are shown as a function of the number of resolutions used and the number of steps involved in the stochastic gradient descent method.

Methods and materials

4D-CT acquisition

Collection of data includes five studies. These are the high-resolution CT scan, 4D-CT, inhalation breath-hold, normal breathing scan, and exhalation breath-hold. Typically, the selection of scan region is dependent on tumor volume and treatment location. For lung, the entire lung volume was acquired. The CT studies were acquired with a pitch of 1.0 and reconstructed in 3 mm slices (1 mm for high resolution scans). The technique selected was the standard chest protocol on a Philips 16-slice Brilliance® CT scanner. Gating was performed with the bellows system, and the phases are selected through automatic increments of 10 % after the user selects the maximum inspiration and end-expiration points of the respiratory cycle.

Landmark intensity variation studies

To investigate the intensity variation in a 4D-CT dataset, a clinic expert manually picked 60 landmarks from each phase of the 4D-CT dataset of a given subject and correlated their HU values. The intensity variations of a set of five

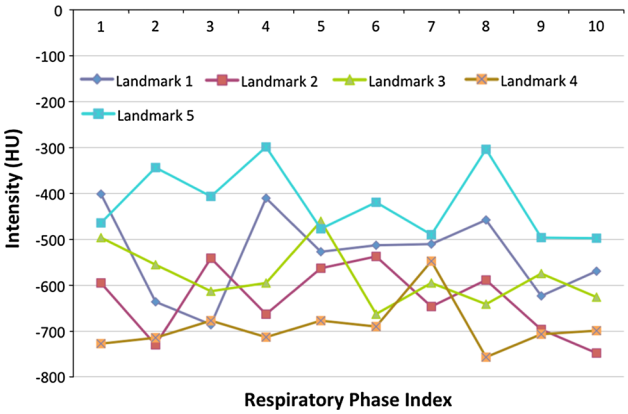

Fig. 1 Landmark intensity variation for landmarks in the left and right lung is shown for *five landmarks*

(among the 60) landmarks are illustrated in Fig. 1. It shows that HU value of a given landmark across different respiratory phases is not constant. In addition, no specific pattern of changes in the HU value was observed. Thus, registration methods that use model-guided estimations of intensity variations [16] may not be applicable with such datasets. To obtain an accurate image-based registration of 4D-CT lungs with optical flow method, the data needed to be conditioned in such a way that the HU values of all anatomical features inside the lung be consistent across the respiratory phases.

4D-CT Lung segmentation

In our approach, we employed multiple anatomical levels, as discussed in "Anatomy level based registration" section, to improve displacement estimation accuracy for voxels that intensity changes. In our approach, we segmented a 3D-CT lung data at multiple anatomical levels based on the anatomy features, as shown in Fig. 2, with all feature points on the same anatomical level assigned to a consistent HU value. The multi-level lung anatomy in our approach was segmented into surface contour, blood vessels, and parenchyma regions. The blood vessel region was segmented into multiple levels according to user specification. Columns of Fig. 2 illustrate four anatomy levels (blood vessel region was further segmented into two levels). Every successive level also includes the anatomy of its previous level with its intensity retained from its previous anatomy level.

Figure 3 shows a segmentation comparison of a left lung CT slice between the two approaches. In the first approach, an intensity threshold was investigated [30]. This was fully automatic approach in which a normalized intensity value was used to separate the blood vessels into multiple levels. Canny edge detector was applied before this segmentation step to obtain the anatomy outline. In the second approach,

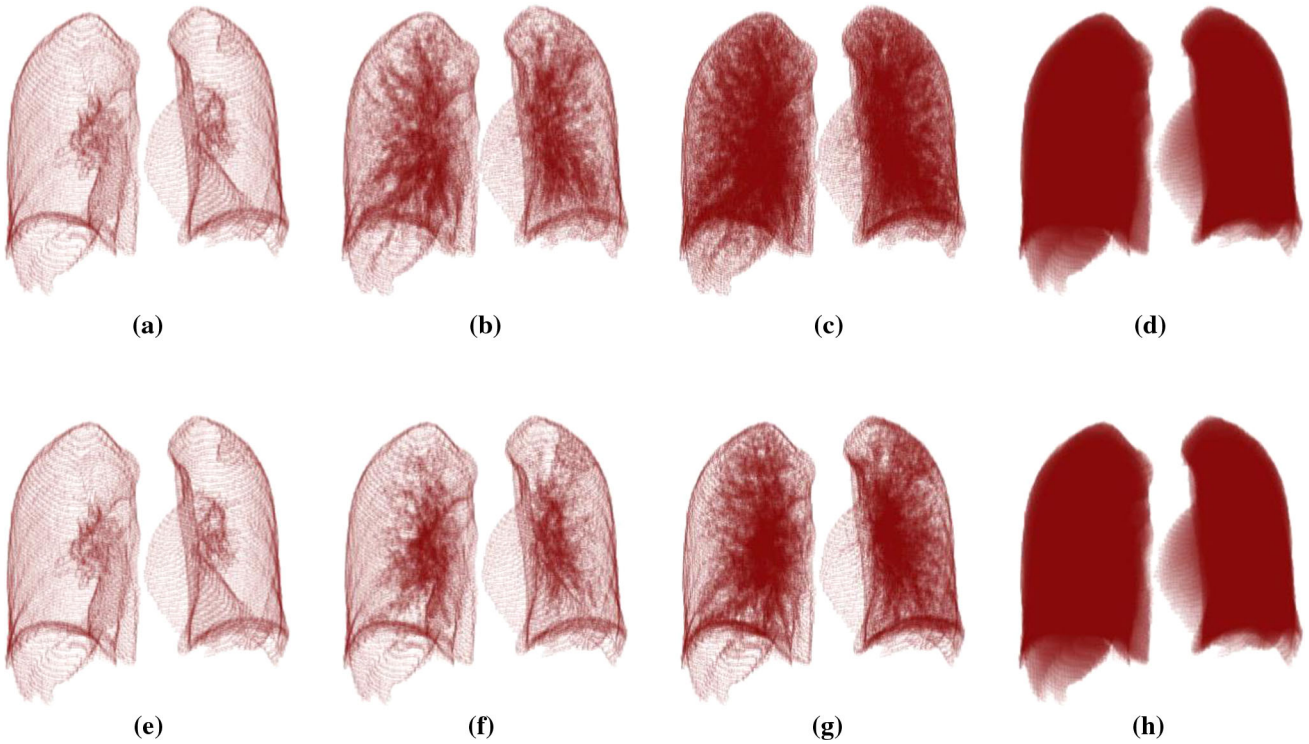

Fig. 2 The accumulated anatomical levels of the lungs, segmented by intensity thresholds approach (**a**–**d**), and seed-based region-growing algorithm (**e**–**h**). The anatomical levels are the **a**, **e** Lung surfaces; **b**, **f** Lung surfaces and large blood vessels; **c**, **g** Lung surfaces, large and small blood vessels; **d**, **h** the whole lungs

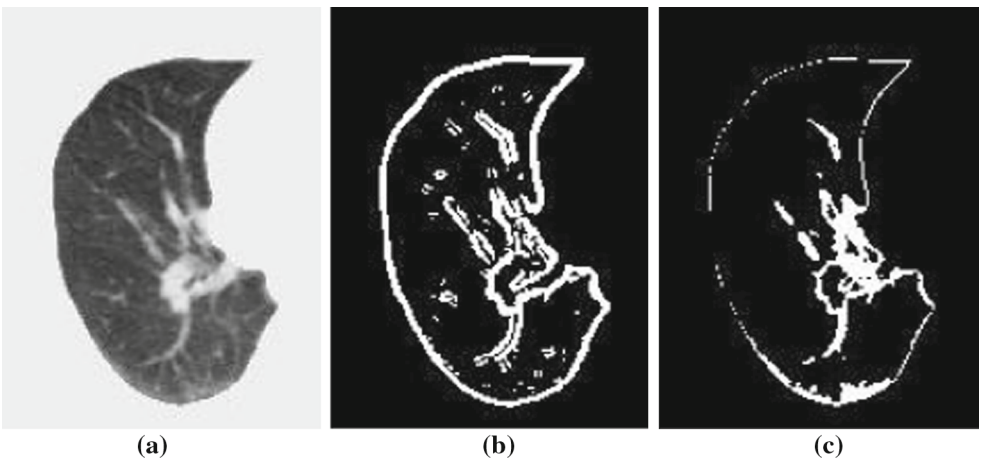

Fig. 3 Comparison between automatic segmentation and semi-automatic segmentation (seed-growing) on 1 subject CT slice. **a** Original CT data, **b** segmented by HU thresholds only **c** segmented by Seed-growing method from multiple manually placed seeds

a semi-automatic seed-based region growth algorithm coupled with a hessian filter was investigated to obtain the blood vessel morphology. The locations of one or more seeds representing the blood vessels were selected on each respiratory phase of a 4D-CT dataset. Using a Hessian filter coupled with a user-defined threshold range, the entire vessel anatomy was segmented. The anatomy was further segmented into multiple levels using blood vessel radius thresholds.

For each of the segmentation approach, the top level (lung surface contour) was segmented from the rest of the lung by its geometry feature—any voxels on the surface of the lung belongs to this anatomical level. The middle anatomical levels (blood vessels) stood out from the bottom anatomy level (parenchyma) by the brighter intensity value. Finally, we unified intensity of a given segmented anatomical level into a constant value.

Proposed optical flow framework

Optical flow registration is based on the observation that the object intensity remains the same during the motion. Therefore,

$$I(x, y, z, t) = I(x + \delta x, y + \delta y, z + \delta z, t + \delta t). \quad (1)$$

Since optical flow registration also assumes the displacement to be small, the relation of displaced location to the original location is unveiled by applying Taylor Series Expansion:

$$I(x + \delta x, y + \delta y, z + \delta z, t + \delta t) = I(x, y, z, t) + \frac{\partial I}{\partial x}\delta x + \frac{\partial I}{\partial y}\delta y + \frac{\partial I}{\partial z}\delta z + \text{H.O.T.} \quad (2)$$

By ignoring higher order terms (H.O.T.), according to Eq. (1),

$$\frac{\partial I}{\partial x}\delta x + \frac{\partial I}{\partial y}\delta y + \frac{\partial I}{\partial z}\delta z = 0. \quad (3)$$

Divide by δt on both side of the Eq. (3),

$$I_x u + I_y v + I_z z + I_t = 0. \quad (4)$$

$I_x I_y I_z$ and I_t and in Eq. (4) stand for the partial derivative of intensity along x, y, z and time dimension separately. At this point, three unknown variables u, v, and w, but only one equation is the optical flow vector. Horn–Schunck method adds an extra constrain to Eq. (4) to solve optical flow motion, which minimize energy function

$$E = \iiint \left[\left(\mathrm{I}_x \mathrm{u} + \mathrm{I}_y \mathrm{v} + \mathrm{I}_z \mathrm{w} + \mathrm{I}_t\right)^2 + \alpha^2 \left(|\nabla u|^2 + |\nabla v|^2 + |\nabla w|^2 \right) \right] \mathrm{d}x\mathrm{d}y\mathrm{d}z. \quad (5)$$

The second part of the function is a smoothness term, α^2 adjusts the weight of smoothness in the global energy function. This function can be minimized with Euler-Lagrange equations.

The displacement for one level is then projected into the next level using TPS as follows: Let x be a vector that represent the voxels at the current anatomical level, who registration is to be performed. Let X be a vector that represents the voxels at the previous anatomical level. The initial displacement for x is computed as

$$u(x(\mathrm{i})) = \sum_{j=0}^{n} \phi(\|x(i) - X(j)\|) u(X(j)), \quad (6)$$

where u stands for estimated initial displacement and ϕ represents the TPS interpolation function. The displacement computed in Eq. (6) is taken as initial displacement for the optical flow analysis for the current level.

It can be seen that the multi-resolution registration of each anatomy level also enables the registration errors in that anatomy level to have minimal effect on the next anatomy level. Once an anatomy level is registered, the registration result is applied to the next anatomy level at the lowest image resolution thereby introducing negligible error for the next anatomy level.

It is to be noted that for an iterative registration algorithm such as the optical flow, the accuracy of the final results strongly rely on the initial value of the displacement [24]. In our proposed work, TPS enabled the displacement computed from one level of anatomy to be propagated to the volume at the next level of anatomy as initial displacement. It is to be noted that the optical flow's smoothness constraint was different from the proposed TPS usage. The final registration was an iterative combination of the multiple anatomical levels and resolutions coupled with TPS, which is the key contribution of the paper.

Workflow

The 3D lung volumes were loaded into the proposed registration system pair by pair. The process is described in Fig. 4.

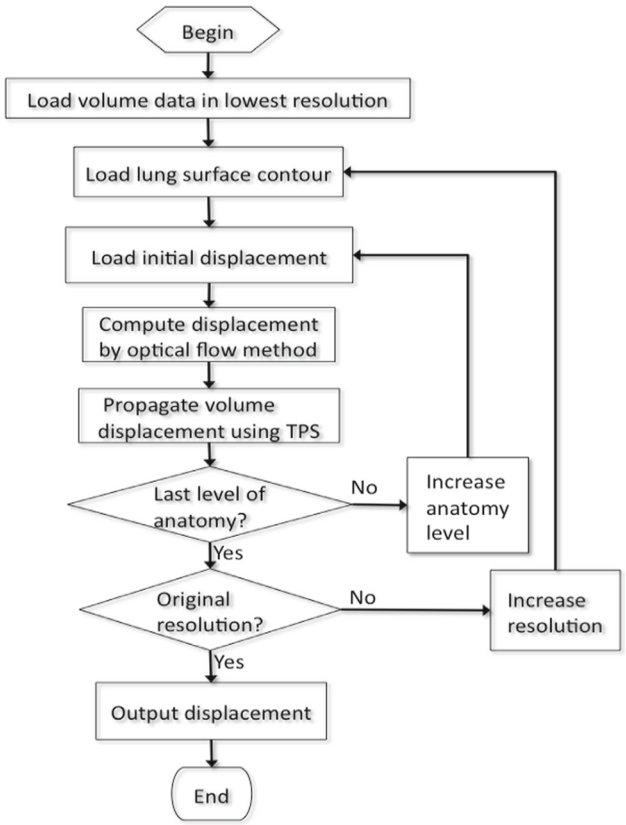

Fig. 4 Flowchart of the proposed MLMR registration method

The 3D volumes at the bottom anatomical level were first computed by rescaling the slices of each volume for each anatomical representation to the lowest resolution. Within each resolution level, the volumes were registered using a multi-anatomical level Horn–Schunck-based optical flow approach. To minimize energy function in Eq. (5) by Horn–Schunck method, the displacement of each voxel was estimated and updated iteratively until global displacement converged or the maximum number of iterations was reached. In each iteration, the displacement was computed as weighted sum of displacements from neighbor voxels, where smoothness factor controlled the magnitude of weight imposed to the point of interest and neighborhood radius defined the range of nearby voxels involved in the calculation. We set smoothness factor to 8.0, neighborhood radius to 5, and use 150 *as the maximum number of* iterations. We found this parameter combination achieved best results for the 4D-CT data we tested. Motion field was first computed based on the pair of surface contours in the lowest resolution. At this stage, all the voxels except those on the surface contour (the lowest level of anatomical representation) were zeros. TPS interpolation was applied to the motion field so that voxels surrounded by the surface contour can have some interpolated motion, which was closer to the actual value. Such motion field was carried as initial motion field to motion computation of the second anatomical level volumes, which now included surface contour and large blood vessels. Care was taken to ensure that the motion field is computed only for the large blood vessels. The motion field was then iteratively updated until the top level of anatomy volumes, which included the surface boundary, large and small blood vessels, and the parenchymal region, was computed by optical flow method and then smoothed by TPS. By this time, the computation of motion field of the volume in lowest resolution was completed. Then, the lung volumes and anatomy maps were rescaled into higher resolution, and the multi-level optical flow registration was performed. Such motion field was iteratively updated until the highest (or original) resolution of the volume was processed. The displacement of each voxel inside the lung was contained in the last updated motion field.

It can be observed that for any given anatomical voxel at a given anatomical level, only its neighborhood points on the same or higher anatomical level contribute to its displacement computing. For instance, when the weighted sum of a voxel in a large blood vessel region was computed, the nearby voxels from either the lung surface contour or the large blood vessel were included, while the rest of neighborhood voxels had no contribution to the voxel being computed. By applying this constraint, errors from low accuracy voxels did not spread to the rest of the region. Thus, the overall accuracy of the method was improved.

Implementation

The automatic system was implemented in MATLAB with OsiriX and ImageJ as segmentation tools. The lung volumes were then exported as CT slices. ImageJ software was then used to semi-automatically find lung contours in each slice and all lung blood vessels by edge detection tools. The intensity unification was performed by setting each segmented anatomical category to a certain intensity value. For instance, voxels on surface contours were set to 255, voxels on large blood vessels are set to 180, small blood vessels are set to 100, and parenchyma regions are set to 0. Such anatomical category marks were saved in images as anatomy maps. The whole lung 4D-CT volume data were read and semi-automatically segmented by two medical experts using open-access segmentation software OsiriX. Validation of the segmentations was done by another clinician using Philips Pinnacle^3 system. The segmentation of the whole lung and its validation were simplified by the fact that the lung boundaries have a very high contrast with its surrounding anatomy.

Validation method

For validation of the optical flow registration method, we used the multi-resolution optical flow registration by Guerrero et al. [10], free-form registration method, inverse consistent demons method, and multi-resolution optical flow registration [31]. The registration methods used for this validation study estimated the displacement map from the end-expiration phase to each of the subsequent phases up to the end-inhalation phase. To establish a ground truth, a set of 60 landmarks, which were the vessel bifurcations, was first manually picked by a clinician through all of the 3D volumes for the respiratory phases. The landmarks' motion estimations using each of the registration methods were then compared with the ground truth motion. The registration accuracy was quantified using TRE and the inverse consistency error with lower error values representing better registration accuracy. The Gamma test has two components: the HU difference and the distance to agreement. The Γ criteria for a particular voxel are found through minimizing Eq. (5), by sampling the reference distribution in the volume surrounding the evaluated voxel [32].

$$\Gamma = \sqrt{\frac{|r_e - r_r|^2}{\Delta r^2} + \frac{(D_e - D_r)^2}{\Delta D^2}}, \tag{7}$$

where Δr and ΔD are the distance to agreement and intensity (HU) difference criteria, r_e and D_e are the position and HU values at the evaluated pixel, and r_r and D_r are the position and HU value of the reference voxel. The acceptance criteria for the Gamma test were set to 1 % intensity differ-

ence range and 2 mm^3 neighborhood range. To account for intensity fluctuations caused by the airflow during the breathing, the multi-level anatomy was used for each landmark. For instance, for a landmark on the vessel bifurcation, an anatomical level that included the lung boundary and blood vessels was only used. The Γ criteria are well within clinical tolerances [33] and were also large enough to avoid statistical aberrations.

Results

In this section, we first present registration results using our proposed method. It is followed by a discussion of the validation studies. Figure 5a, c represents as overlapping 2D slices of left lung and right lung at end-exhalation (red) and end-inhalation (green) stages. The misalignments between each of the slices are depicted in red and green colors. While the red region represents the features that are in the end-exhalation and not in end-inhalation, the green region represents the features that are in the end-inhalation and not in the end-exhalation. Overlapping the warped image with the target image where the red and green colors are not seen represents a correct image registration. Figure 5b, d represents the overlapping 2D slices of the left and right lung with the end-inhalation lung volume warped using the registration results. It can be visually seen that the registration error is minimal for each of the case.

Validation studies are presented for a set of 4D-CT datasets with each datasets having 60 landmarks for each of the lung volumes. Additionally, to quantify the usage of such a registration, we used two comparisons: (a) we investigated the multi-level registration without the inclusion of TPS as a comparison and (b) we varied the number of anatomical levels to observe the improvement in the registration results.

Table 1 shows the TRE estimation for a set of five subjects when the landmarks are tracked between 0 % inhalation to 30 % inhalation phase, 0–60 % inhalation phase, and 0–100 % inhalation phase, respectively; 0 and 100 % inhalation means the beginning and end of inhalation cycle, respectively; 30 and 60 % inhalation were the respiratory phases in the middle of inhalation cycle. The percentages of air volume intake were provided by the gated CT acquisition system. Four different registration approaches were investigated in conjunction with three segmentation methods. The "No Segmentation" method represents the optical flow-based registration method without anatomical segmentation involved, to give quantitative comparison of the anatomical segmentation contribution in the purposed MLMR method. In the first case, three levels of anatomical representation were used along with the TPS. The three levels of anatomical representation for the three subjects included the lung surface, lung surface together with the large blood vessels, and the combination of lung surface, large and small blood vessels. In this case, the HU values in the parenchymal region were unified to 0, and therefore, parenchymal region was not directly included during the optical flow computation. It can be seen that for the first subject, the TRE had a mean of 3.00 mm with a standard deviation of 3.33 mm for the case of 0 % inhalation volume registered with 100 % inhalation volume. For the second subject, a mean TRE of 2.84 mm with a standard deviation of 2.27 mm was obtained. When the parenchymal region is considered as an additional anatomical level (for four total anatomical levels), HU values in the parenchymal region were counted without unifying to 0,_along with TPS, the TRE increases to a mean of 4.59 mm with a standard deviation of 4.49 mm for the first subject and to a mean of 3.76 mm with a standard deviation of 2.71 mm. This was because of the low contrast in the intensity for the parenchymal region. When the registration was performed without the

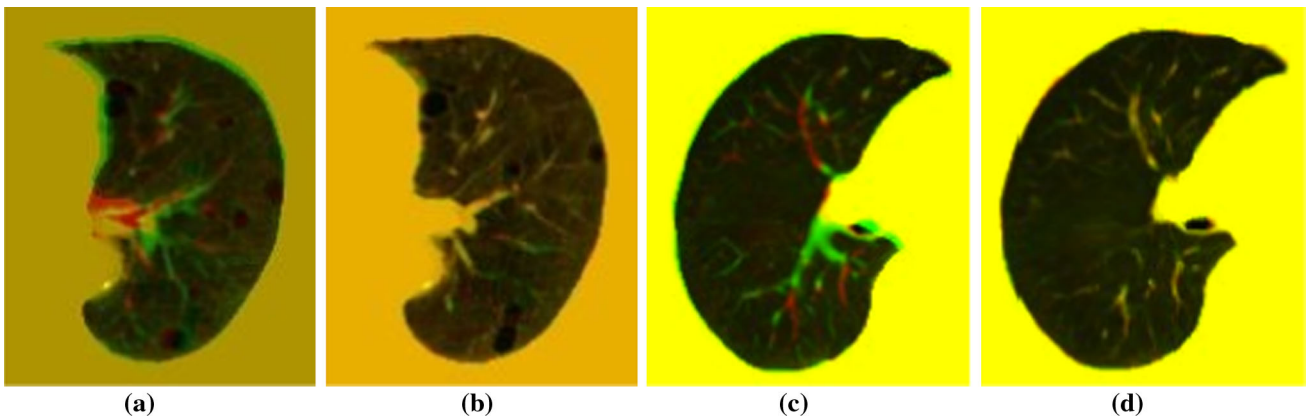

Fig. 5 The 2D lung slices of two right lung volumes at end-expiration (*red*) and end-inspiration (*green*) are shown **a** before and **b** after the registration. The 2D lung slices of two left lung volumes at end-expiration (*red*) and end-inspiration (*green*) are shown **c** before and **d** after the registration. The misalignments for each of the case are depicted in *red* and *green* colors

Table 1 TRE comparison of MLMR with different configuration and multi-resolution method (unit: mm)

Segmentation method	Optical flow registration method	Respiratory phase pair	Subject 1		Subject 2		Subject 3		Subject 4		Subject 5	
			Mean	STD	Mean	STD	Mean	STD	Mean	STD	Mean	STD
Intensity threshold	MLMR 3 level	0–30 % inhalation	1.84	1.17	2.06	1.50	1.81	1.41	1.58	1.09	1.39	1.0
	MLMR 4 level		1.83	1.27	1.96	1.84	1.55	1.45	1.49	0.98	1.61	0.8
	MLMR 4 level no		1.95	1.22	2.53	1.94	1.85	1.40	1.84	1.58	2.12	1.48
Single-level seed-growing algorithm	MLMR 3 level		2.00	1.29	2.35	1.47	1.91	1.36	2.38	1.17	2.38	0.72
	MLMR 4 level		1.98	1.27	2.09	1.73	1.68	1.45	1.78	1.2	1.91	0.86
	MLMR 4 level no		2.03	1.38	2.57	1.79	1.74	1.53	2.07	1.75	2.15	1.66
Double-level seed-growing algorithm	MLMR 3 level		2.02	1.36	2.42	1.40	1.83	1.33	2.26	0.97	2.31	1.34
	MLMR 4 level		1.96	1.17	2.26	1.73	1.66	1.39	1.27	1.42	1.36	1.53
	MLMR 4 level no		2.23	1.30	3.07	2.02	1.91	1.34	2.35	1.41	2.67	1.89
No segmentation	Multi-resolution		2.03	1.32	2.30	1.84	1.68	1.37	1.56	1.61	1.65	1.21
Intensity threshold	MLMR 3 level	0–60 % inhalation	2.16	1.66	2.31	1.86	2.67	3.23	3.08	3.7	2.69	3.7
	MLMR 4 level		2.70	2.18	2.76	2.33	3.77	3.97	3.83	4.31	3.87	3.96
	MLMR 4 level no		3.55	2.88	3.09	2.75	4.11	4.24	4.42	4.13	4.51	4.26
Single-level seed-growing algorithm	MLMR 3 level		2.62	1.80	3.04	2.03	3.30	3.09	3.56	2.98	3.65	2.57
	MLMR 4 level		3.15	2.40	2.79	2.13	4.08	4.27	3.75	4.43	3.58	4.31
	MLMR 4 level no		3.64	2.82	3.46	2.54	5.20	4.99	4.83	5.32	5.3	5.41
Double-level seed-growing algorithm	MLMR 3 level		2.55	1.79	3.00	1.98	3.43	3.02	3.34	3.48	3.39	3.65
	MLMR 4 level		3.23	2.44	2.84	2.19	3.76	3.89	3.48	4.2	3.68	4.59
	MLMR 4 level no		3.54	2.71	3.38	2.95	5.33	5.02	5.31	4.84	4.97	4.95
No segmentation	Multi-resolution		4.03	3.02	3.40	2.72	4.96	4.35	4.51	4.81	4.79	4.41
Intensity threshold	MLMR 3 level	0–100 % inhalation	3.00	3.33	2.84	2.27	2.78	3.25	2.93	2.85	2.44	2.44
	MLMR 4 level		4.59	4.49	3.76	2.71	4.89	4.28	4.6	4.77	4.52	5.21
	MLMR 4 level no		5.34	4.17	4.25	3.10	5.10	4.54	5.02	4.18	4.79	4.6
Single-level seed-growing algorithm	MLMR 3 level		3.62	3.35	4.19	2.55	4.30	3.08	4.34	3.14	4.75	2.89
	MLMR 4 level		4.98	4.25	4.66	2.65	5.86	4.39	6.23	4.8	6	4.51
	MLMR 4 level no		5.74	4.63	5.05	3.22	7.50	4.87	7.8	5.31	8.29	5.4
Double-level seed-growing algorithm	MLMR 3 level		3.53	3.33	4.33	2.66	4.32	3.10	4.27	2.86	4.7	2.65
	MLMR 4 level		4.73	4.08	4.24	2.51	5.43	4.08	5.85	3.98	5.76	3.73
	MLMR 4 level no		5.58	4.68	5.62	3.58	7.77	5.20	7.88	5	8.24	5.45
No segmentation	Multi-resolution		6.67	4.82	4.80	3.32	6.90	5.46	6.65	5.28	6.52	5.65

usage of TPS, the mean TRE for the first subject was 5.34 mm with a standard deviation of 4.17 mm and the mean TRE for the second subject was 4.25 mm with a standard deviation of 3.10 mm. Thus, for registering the parenchymal region, the thin-plate splines showed an improved accuracy as compared to optical flow registration. When compared with the results obtained from multi-resolution optical flow, the mean TRE for the first subject was 6.67 mm with a standard deviation of 4.82 mm and mean TRE for the second subject was 4.80 mm with a standard deviation of 3.32 mm. Similar results were observed for all the three subjects supporting the observation that the proposed MLMR optical flow registration with three levels of anatomy provides a TRE <3 mm.

The mean and standard deviation of the TRE is tabulated in Table 2 for each of the methods considering all the lung volumes of each of the 4D-CT datasets. When look into TRE of subject 5, it can be seen that the MLMR optical flow with 3 levels of anatomy provides a mean TRE of 2.25 mm. When compared with multi-resolution optical flow method with the TRE of 6.93 mm and non-optical flow methods (free-form and inverse consistent demons) with the TRE of 16.90 and 8.11 mm, respectively, the proposed method yielded an accurate 4D-CT registration. Such variations in the result can be attributed to the landmark intensity inconsistency issue inherent in the 4D-CT datasets. In addition, although all the registration methods were used on MATLAB, we implemented MLMR and multi-resolution registration methods and obtained the implementation of free-form and inverse consistent demon methods through DIRART software suite [31].

For a qualitative evaluation of the lung inhalation and exhalation, we performed a Jacobian analysis. The mean of

Table 2 TRE comparison for MLMR and other methods for 10 volumes of 4D-CT datasets (unit: mm)

Method	Subject 1		Subject 2		Subject 3		Subject 4		Subject 5	
	Mean	STD	Mean	STD	Mean	STD	Mean	STD	Mean	STD
MLMR 3 levels TPS	2.28	1.25	2.25	1.56	2.93	2.78	1.79	1.44	2.25	2.21
MLMR 4 levels TPS	3.15	3.68	2.94	2.05	4.51	3.72	2.50	2.31	3.82	3.02
MLMR 4 levels no TPS	4.25	4.05	3.61	2.37	4.93	3.99	3.80	2.99	5.92	3.52
Multi-resolution optical flow	5.06	4.43	4.35	3.50	5.40	4.34	4.68	3.60	6.93	3.81
Free-form deformation	22.96	5.68	10.89	4.44	16.50	5.35	11.28	5.00	16.90	6.87
Inverse consistent demons	11.19	3.98	5.13	2.60	7.41	4.93	5.13	4.46	8.11	4.35

Table 3 Mean of the Jacobian comparison for the MLMR and other registration

Subject	Lung side	Inhalation phase (%)	MLMR optical flow 3 levels TPS	MLMR optical flow 4 levels TPS	MLMR optical flow 4 levels no TPS	Multi-resolution optical flow	Free-form deformation method	Inverse consistent demons method
Subject 1	Left	0–30	1.0232	1.0282	1.0289	1.034	1.01	0.9714
		0–60	1.142	1.1409	1.1394	1.1412	1.0259	0.9596
		0–100	1.1898	1.1907	1.1961	1.2297	1.0168	0.9665
	Right	0–30	1.0312	1.0391	1.039	1.0458	0.8965	0.958
		0–60	1.1277	1.1397	1.1449	1.2144	0.95	0.9256
		0–100	1.1715	1.2092	1.2455	1.2921	0.98	0.9505
Subject 2	Left	0–30	0.97	0.9569	0.9529	0.9658	1.0927	1.036
		0–60	1.044	1.0525	1.0512	1.12	0.9972	0.9987
		0–100	1.0598	1.0872	1.0842	1.6526	0.997	1.0165
	Right	0–30	0.9722	0.9724	0.9734	0.9571	1.008	1.0348
		0–60	1.0391	1.0673	1.0661	1.065	0.9092	0.9802
		0–100	1.0477	1.0788	1.0782	1.064	0.94	0.9733
Subject 3	Left	0–30	1.009	1.0211	1.02	1.0236	0.9557	0.9724
		0–60	1.0693	1.131	1.1302	1.1153	0.9613	0.9214
		0–100	1.0967	1.183	1.1906	1.2932	0.9646	0.9307
	Right	0–30	1.0199	1.0224	1.0187	1.0268	0.98	0.9798
		0–60	1.0759	1.1319	1.1328	1.1328	0.8929	0.9304
		0–100	1.1054	1.1693	1.1698	1.5978	0.9078	0.9159
Subject 4	Left	0–30	1.012	1.0532	1.05	1.0623	1.043	1.0653
		0–60	1.093	1.163	1.1633	1.1853	1.082	1.0993
		0–100	1.117	1.209	1.2226	1.3232	1.134	1.122
	Right	0–30	1.023	1.0532	1.0212	1.0668	1.002	1.043
		0–60	1.0799	1.1673	1.1658	1.1248	1.075	1.0802
		0–100	1.1402	1.1924	1.1933	1.6278	1.143	1.129
Subject 5	Left	0–30	1.01	1.0421	1.04	1.05	1.037	1.074
		0–60	1.081	1.147	1.143	1.1673	1.094	1.135
		0–100	1.102	1.189	1.2114	1.3193	1.145	1.167
	Right	0–30	1.011	1.0416	1.017	1.0475	1.002	1.067
		0–60	1.0659	1.1527	1.1523	1.1195	1.114	1.096
		0–100	1.1202	1.1811	1.1873	1.3245	1.178	1.125

the Jacobian was computed using DIRART software suite and is tabulated in Table 3 for each of the methods. The Jacobian determinant value was positive and increased as the lung volume increased for each of the methods. However, the inconsistent intensity value introduced errors in the non-optical flow methods' displacement estimation that caused inconsistency in the correlations of the Jacobian value. The multi-resolution optical flow method yielded a better consis-

Table 4 Inverse consistency error for the proposed MLMR optical flow with three levels of anatomy and TPS-based propagation (unit: mm)

Inhalation	Subject 1		Subject 2		Subject 3		Subject 4		Subject 5	
	Left	Right	Left	Right	Left	Right	Left	Right	Left	Right
0–30 %	1.43	1.23	1.11	1.08	0.73	1.18	1.12	0.97	1.67	1.04
0–60 %	2.89	2.73	1.51	1.15	2.35	1.9	1.48	1.02	1.83	1.19
0–100 %	3.58	3.3	2.37	1.74	3.1	2.2	2.24	1.37	2.02	1.67
Average	2.63	2.42	1.66	1.32	2.06	1.76	1.61	1.12	1.84	1.30

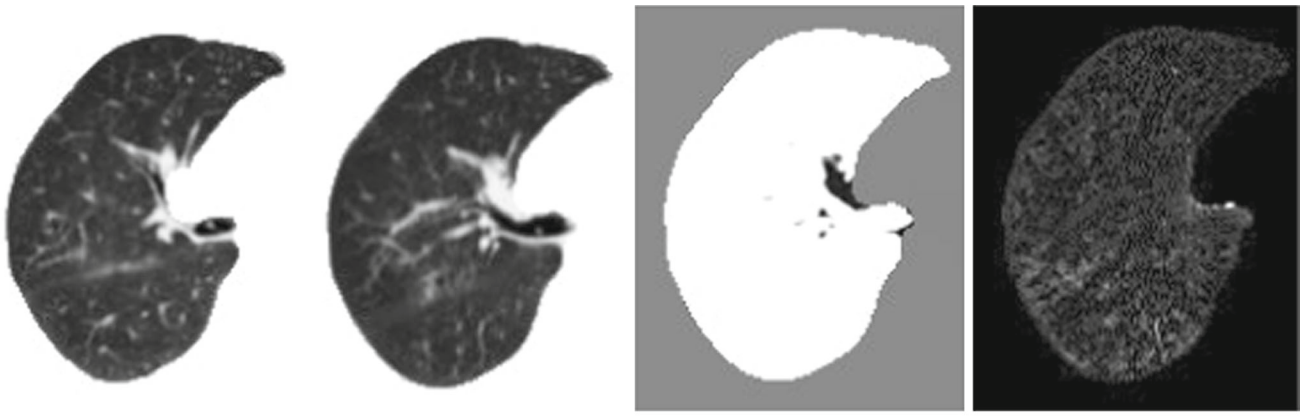

(a) **(b)** **(c)** **(d)**

Fig. 6 2D slice representation of the left lung at **a** end-exhalation and **b** end-inhalation

Table 5 Percentage voxels that fail the gamma statistics

Inhalation	Subject 1		Subject 2		Subject 3		Subject 4		Subject 5	
	Left	Right	Left	Right	Left	Right	Left	Right	Left	Left
0–30 %	1.94	0.40	1.69	0.72	0.17	1.29	0.24	1.50	1.62	1.94
0–60 %	2.50	1.12	2.65	1.67	0.58	2.25	0.57	2.30	1.99	2.50
0–100 %	2.92	1.27	2.77	1.68	1.51	3.14	1.16	2.59	2.44	2.92
Average	2.45	0.93	2.37	1.35	0.75	2.23	0.66	2.13	2.02	2.45

tency in the linear correlations of the Jacobian value because of its smoothening component. The proposed method yielded results that showed a more consistent linear increase in the Jacobian value.

Table 4 shows the inverse consistency results for the five 4D-CT datasets. In this context, the term consistency refers to the difference between the positions of the source lung volume and the target lung volume that was warped using the inverted displacement vectors that were originally calculated to warp the source lung volume to target lung volume. A three level anatomy with TPS for parenchymal registration was used for this analysis. Two displacements for each subject are computed registering the source 3D-CT with target 3D-CT and registering the target 3D-CT with the source 3D-CT, and then the two displacements are compared to calculate the consistency error. It can be seen that the proposed method has a consistency error in the range of 0.7–3.6 mm.

Figure 6 presents the gamma results (discussed in "Validation method" section) for a lung slice. Figure 6a, b represents the 2D anatomy at end-exhalation and end-inhalation breathing phases. Figure 6c presents the voxel distribution that fail the gamma criteria when end-exhalation and end-inhalation are used. Figure 6d presents the voxel distribution that fails the gamma criteria when the end-exhalation is warped using the registration results and compared with the end-inhalation breathing phase image. It can be seen that very small number of voxels fails the criteria after registration. Table 5 presents the gamma statistics between two 4D-CT volumes. In each case, the lung volume at 30 % inhalation phase is warped using the registration results to fit the lung volume at 0 % inhalation phase. Results show that using the proposed registration framework, the percentage of voxels in the warped lung volume that fail the gamma criteria is <3 %. The average number of voxels that failed the gamma criteria was also

Table 6 Run-time statistics for a pair of respiratory phases (Data size: 512 × 512 × 128 voxel)

Machine configuration		MLMR configuration			Time (min)
CPU (GHz)	RAM (GB)	Smoothness	Neighborhood	Iteration	
Intel Core 2 Duo 2.16	4	8.0	5 voxels	150	20
Intel Core i5 2.6	4	8.0	5 voxels	150	17

<3 %. The 3 % mismatch in the gamma criteria was a result of the inconsistencies in the intensity of corresponding voxels between the source and the target volumes.

Table 6 presents the run-time statistics. The MATLAB implementation of the proposed algorithm took approximately 20 and 17 min on two different configurations, respectively.

The voxels in this 2D slice that failed the criteria are colored in white, while the voxels that passed the Γ criteria are colored in dark. The gamma statistics before and after the registration are shown in (c) and (d), respectively.

In summary, the usage of MLMR optical flow with three levels of anatomy and TPS to propagate the results, from one anatomical level to another, yielded a minimal TRE for each of the five 4D-CT volume datasets, as well as the overall dataset. Additionally, the maximum landmark error was also shown to be minimal as compared to both multi-resolution optical flow method as well as non-optical flow methods. The inverse consistency of the displacements was also shown to be <2 mm. Finally, the gamma statistical analysis also supports the clinical applicability of the registration method discussed in this paper. Such result shows that the proposed method facilitates a 4D-CT registration with higher accuracy.

Discussion

In this paper, we present a multiple anatomical levels and multiple resolutions optical flow method for registering 4D-CT lung respiratory phases. The proposed method enabled us to compute the volumetric lung displacement, a key parameter in estimating the 3D elasticity of each subject's lung-thereby allowing the usage of physics-based volumetric lung deformations during lung radiotherapy.

Inconsistent intensity for lung anatomical structures in a 4D-CT image may have been brought by lung motion and large air volume change inside the lung during respiration. Such variations may be very high as observed in the case of 4D-CT lung image datasets acquired at our institution for non-small-lung cancer subjects. In the proposed work, we addressed the issue by unifying the intensity of a specific sub-anatomy to a constant value on all lung respiratory phases. The anatomical segmentations were performed using two approaches, namely the intensity gradient threshold approach and seed-based region growth algorithm. The proposed registration method was both multi-anatomy level and multi-resolution, i.e., the final displacement of the entire lung volume at one resolution level is propagated as initial displacement for the next resolution level.

In 4D-CT image datasets, it can be observed that voxels representing different lung sub-anatomy have feature intensities in the same range or close to noise intensity. Displacement estimation in such regions using 4D-CT registration techniques may be inaccurate when intensity-based registration methods are employed. However, features in lung contour and regions around blood vessels were quite easily distinguished, as they tend to have high intensity contrast. Displacement estimations were accurate in these regions. The multi-level nature of the proposed registration method first groups voxels into several anatomical levels based on the lung sub-anatomic representation. When compared with multi-resolution optical flow, the proposed method was able to better account for non-constant intensity of landmarks and low contrast that are inherent in the input dataset.

The usage of TPS along with the optical flow also raised the issue of whether the optical flow registration be used for registering parenchymal regions, where the landmark intensity contrast is very low. Results discussed in the proposed work (Table 1) quantified the effect of such errors from one resolution level to another by computing the final validation difference. It can be seen that when the TPS was not used, the registration error was higher as compared to the case when the TPS was used without making any modifications to the optical flow smoothening constraint.

The validation study of MLMR registration method involved two clinical experts to carefully mark 60 landmarks for each respiratory phase in the lung. We then compared with other registration methods especially the methods from DIRART package. As registration accuracy highly depends on registration parameter setting, patient breathing displacement pattern, and 4D-CT image quality, huge registration accuracy differences were observed for the same registration method over multiple datasets. For instance, while optical flow registration method achieves a TRE of 1.6 ± 0.9 mm with datasets acquired in Latifi et al. [34], it presented a higher registration error with our datasets. Public datasets from POPI-model [35] or EMPIRE10 framework [36] enable a common platform to investigate the registration accuracy

as a relation to the registration parameters. Future work will investigate the optimal registration parameter set for each registration mechanism and how it will be applicable for 4D CT datasets generated by other non-public datasets.

The HAMMER algorithm has been proposed as a hierarchical approach for brain image registration [26,27], but differs from the proposed algorithm. From implementation perspective: (a) the HAMMER algorithm used the forward and backward propagation matching for registering the sparse set of landmarks for three anatomical levels inside the brain. The rest of the pixels were registered using TPS. Our proposed method registers anatomical levels from sparse to dense using a multi-resolution optical flow approach. On each resolution level, TPS was employed only to propagate the displacement to carry to the next resolution level; (b) The HAMMER algorithm has been employed with three fixed anatomical levels. Our proposed method addressed the knowledge-gap of how many anatomical levels were required for an improved registration. We have employed three and four anatomical levels to address the question as to whether the accuracy improves with an increase in the number of levels. Additionally, we have presented results in "Results" section on whether the accuracy changes when the TPS was not employed. Thus, the proposed work also addressed a key knowledge-gap on the relation between the number of hierarchical levels required for the registration and the accuracy of the registration itself. From medical image perspective: (a) The HAMMER algorithms have not been investigated by peers for the 4D-CT lung registration problem to our knowledge; (b) The lung anatomy, which is the focus of our problem, expands and contracts during breathing. Our registration method focused on registration of four levels of landmarks taking into account the presence of breathing-induced artifacts. Thus, the proposed method shows feasibility of using hierarchical attribute-based registration for lung datasets when the local anatomy undergoes changes from one air volume to another.

The estimated lung displacement was observed to be heterogeneous from one respiratory phase to another. In other words, the amount of voxel displacement varied for a given voxel from one respiratory phase to another. Additionally, it can also be seen that the displacement itself varied from one 4D-CT dataset to another. Such variations in the lung displacement further emphasized the need for subject-specific physics-based deformation models.

Future work will better shed light on the radiotherapy treatment efficacy and the accuracy of the lung registration on a subject-by-subject basis. This will be achieved in two steps. First, from a radiotherapy perspective, the registration results from three variants of the proposed registration framework and the method discussed by Guerrero et al. [10] will be used to simulate the radiation dose delivery on three different subjects. The radiation dose delivery simulation method that takes into account the subject-specific lung motion has been previously discussed in [37]. Results in terms of the dose-volume histograms (DVH) for the dose delivered to the tumor will show the significance of the 1–3 voxel error on the overall treatment dose delivered. Such an analysis will show whether significant difference in the DVH of the dose simulation is observed when the displacement obtained from the different registration methods is used. Such differences will also suggest whether a small improvement in the registration accuracy can be observed to be significant for radiotherapy-based clinical cases. Second, the registration results will be used to estimate the Young's Modulus (YM), a tissue elastic property, associated with each lung voxel. The method of estimating the YM for each voxel has been previously discussed in Santhanam et al. [38]. Results will further show whether subtle variations in the registration can lead to significant variations in the YM associated with each voxel. Developing such physics-based models also enables to iteratively improve 4D CT image registration by including physics-based phenomenon such as airflow inside lungs and interface slippage, both of which can significantly improve the 4D CT lung registration process.

The proposed method was based on the segmentation of the lung anatomy at different levels of representation. The accuracy of the proposed method was thus dependent upon the accuracy of the segmentation procedure. In the proposed work, we have employed an open-access image processing software, OsiriX, based automatic segmentation of the lung anatomy and a seed-based region growth algorithm for manual segmentation for the lung anatomy. The effort involved in such a multi-level anatomical segmentation was minimal for lung anatomy. However, complex model-based segmentations can be used to further improve the segmentation accuracy and subsequently the registration accuracy. Future work will focus on the usage of different automatic and manual segmentation methods and their effect on the accuracy of the registration procedure. In addition, future work will also focus on minimizing the changes in the voxel intensity of landmarks during image acquisition without exposing the subject to more radiation during imaging.

The inverse consistent analysis was only used as one of the metrics for evaluating our registration accuracy. In the future work, we will include the inverse consistency on each anatomy level in our registration method as well. Such a registration would significantly increase the registration computation time. We will employ state-of-the-art GPU cluster to improve the computation speed and better facilitate such a registration mechanism.

For performance comparison purposes, we used a multi-resolution optical flow, free-form method, and inverse consistent demons methods. Results show variations in the TRE for each of the methods. Also, it can be seen that methods that were not based on multi-resolution provide a larger

TRE value as the variations in the voxel intensities from one volume to another add more uncertainty in the registration process. Additional validation metrics such as ICE and the gamma statistical analyses showed that the proposed registration was able to achieve a registration accuracy that will be applicable for radiotherapy needs.

Future work will focus on benchmarking the registration accuracy using lung datasets with minimal inaccuracies and improving the accuracy using additional image-based constraints such as multi-level contrast and physics-based constraints such as airflow modeling. The use of graphics processing units will also be investigated for addressing real-time computational requirements.

Acknowledgments This project is supported in part by James and Esther King Grant Florida, National Science Foundation (1200579), and the University of California, Los Angeles.

Conflict of interest Yugang Min, John Neylon, Amish Shah, Sanford Meeks, Percy Lee, Patrick Kupelian and Anand P. Santhanam declare no conflict of interest.

References

1. Keall PJ, Mageras GS, Balter JM, Emery RS, Forster KM, Jiang SB, Kapatoes JM, Low DA, Murphy MJ, Murray BR, Ramsey CR, van Herk MB, Vedam SS, Wong JW, Yorke E (2006) The management of respiratory motion in radiation oncology report of AAPM Task Group 76. Med Phys 33(10):3874–3900
2. Bortfeld T, Jiang SB, Rietzel E (2004) Effects of motion on the total dose distribution. Semin Radiat Oncol 14(1):41–51
3. Starkschall G, Britton K, McAleer MF, Jeter MD, Kaus MR, Bzdusek K, Mohan R, Cox JD (2009) Potential dosimetry benefits of four-dimensional radiation treatment planning. Med Phys 73(5):1560–1565
4. Vinogradskiy YY, Balter P, Followill DS, Alvarez PE, White RA, Starkschall G (2009) Comparing the accuracy of 4D photon dose calculation with 3D calculating using moving and deforming phantoms. Med Phys 36(11):5000–5006
5. Vinogradskiy YY, Balter P, Followill DS, Alvarez PE, White RA, Starkschall G (2009) Verification of four dimensional dose calculations. Med Phys 36(8):3438–3447
6. McClelland JR, Hughes S, Modat M, Qureshi A, Ahmad S, Landau D, Ourselin S, Hawkes DJ (2011) Inter-fraction variations in respiratory motion models. Phys Med Biol 56(2011):251–272
7. Metaxas DN (1996) Physics-based deformable models: applications to computer vision, graphics, and medical imaging, 1st edn. Kluwer Academic Publishers Norwell, MA
8. Santhanam AP, Willoughby T, Shah A, Meeks SL, Rolland JP, Kupelian P (2008) Real-time simulation of 4D lung tumor radiotherapy using a breathing model. Lect Notes Comput Sci 2:710–717
9. Klinder T, Lorenz C, von Berg J, Renisch S, Blaffert T, Ostermann J (2008) 4DCT image-based motion field extraction and analysis. In: SPIE Medical, Imaging. SPIE
10. Guerrero T, Sanders K, Castillo E, Zhang Y, Bidaut L, Pan T, Komaki R (2006) Dynamic ventilation imaging from four-dimensional computed tomography. Phys Med Biol 51(4):777–791
11. Zhang GG, Huang T-C, Guerrero T, Lin K-P, Stevens C, Starkschall G, Forster K (2008) Use of three-dimensional optical flow method in mapping 3D anatomic structure and tumor contours across four-dimensional computed tomography data. J Appl Clin Med Phys 9(1):2738
12. Brock KK (2007) A multi-institution deformable registration accuracy study. Int J Radiat Oncol Biol Phys 69(3):S44
13. Sarrut D, Boldea V, Ayadi M, Badel J-N, Gineset C, Clippe S, Carrie C (2005) Non-rigid registration method to assess reproducibility of breathing-holding with ABC in lung cancer. Int J Radiat Oncol Biol Phys 61(2):594–607
14. Murphy K, van Ginneken B, Pluim JPW, Klien S, Staring M (2008) Quantitative assessment of registration in thoracic CT. In: First international workshop on pulmonary image processing. pp 203–211
15. Betke M, Hong H, Thomas D, Chekema P, Ko JP (2003) Landmark detection in the chest and registration of lung surfaces with an application to nodule registration. Med Image Anal 7:265–281
16. Yin Y, Hoffman EA, Lin CL (2009) Mass preserving non-rigid registration of CT lung images using cubic b-spline. Med Phys 36(9):4213–4222
17. Fan L, Chen CW (1999) 3D warping and registration from lung images. In: Medical Imaging. SPIE, pp 459–470
18. Fan L, Chen CW, Reinhardt JM, Eric AH (2001) Evaluation and application of 3D lung warping and registration model using HRCT images. In: Medical Imaging. SPIE, pp 234–243
19. Christensen GE, Song JH, Lu W, Naga IE, Daniel AL (2007) Tracking lung tissue motion and expansion/compression with inverse consistent image registration and spirometry. Med Phys 34(6):2155–2167
20. Christensen GE, Johnson H (2001) Consistent image registration. IEEE Trans Med Imaging 20(7):568–572
21. Christensen GE (2005) Inverse consistent image registration. In: Handbook of biomedical image analysis vol III. pp 219–250
22. Ding K, Cao K, Christensen GE, Raghavan ML, Hoffman EA, Reinhardt JM (2008) Registration based lung tissue mechanics assessment during tidal breathing. In: Medical Image Analysis. Lecture notes on computer science, pp 63–72
23. Pan Y, Kumar D, Hoffman EA, Christensen GE, Mclennan G, Song JH, Ross A, Simon BA, Reinhardt JM (2005) Estimation of regional lung expansion via 3D image registration. In: Medical, Imaging. SPIE
24. Horn BKP, Schunck BG (1981) Determining optical flow. Artif Intell 17:185–204
25. Lorenzen P, Davis B, Shen J (2004) Model-based symmetric information theoretic large deformation multi-modal image registration. In: International symposium of Biomedical Imaging. pp 72–723
26. Wu G, Yap P, Kim M, Shen D (2010) TPS-HAMMER: Improving HAMMER registration algorithm by soft correspondence matching and thin plate splines based deformation interpolation. NeuroImage 49:2225–2233
27. Shen D, Davatzikos C (2002) HAMMER: Hierarchical attribute matching mechanism for elastic registration. IEEE Trans. Med. Imaging 21(11):1421–1439
28. Wu G, Wang Q, Lian J, Shen D (2011) Re-construction of 4D-CT from a single free-breathing 3D-CT by spatial temporal image registration. In: Information Processing in Medical Imaging. pp 686–698
29. Vik T, Kabus S, von Berg J, Ens K, Dries S, Klinder T, Lorenz C (2008) Validation and comparison of registration methods for free-breathing 4D lung-CT. In: Medical, Imaging. SPIE
30. Pflicke H, Sixt M (2009) Preformed portals facilitate dendritic cell entry into afferent lymphatic vessels. J Exp Med 206(13):2925
31. Yang D, Brame S, El Naqa I, Aditya A, Wu Y, Goddu SM, Mutic S, Deasy JO, Low DA (2010) DIRART-a software suite for deformable image registration and adaptive radiotherapy research. Med Phys 30(1):67–77
32. Low D (2010) Gamma dose distribution evaluation tool. Journal of Physics conference series (250)

33. Fraass B, Doppke K, Hunt M, Kutcher G, Starkschall G, Stern R, Van Dyke J (1998) American association of physicists in medicine radiation therapy committee task group 53: quality assurance for clinical radiotherapy treatment planning. Med Phys 25(10):1773–1829
34. Latifi K, Zhang G, Stawicki M, van Elmpt W, Dekker A, Forster K (2013) Validation of three deformable image registration algorithms for the thorax. J Appl Clin Med Phys 14(1):3834
35. Vandemeulebrouche J, Sarrut D, Clarysse P (2007) The POPI-model, a point-validated pixel-based breathing thorax model. International Conference on the Use of Computers in Radiation Therapy
36. Murphy KJ, van Ginneken B, Reinhardt JM, Kabus S, Ding K, Deng X, Cao K, Du K, Christensen GE, Garcia V, Vercauteren T, Ayache N, Commowick O, Malandain G, Glocker B, Paragios N, Navab N, Gorbunova V, Sporring J, de Bruijne M, Han X, Heinrick MP, Schnabel JA, Jenkinson M, Lorenz C, Modat M, McClelland JR, Ourselin S, Muenzing SEA, Viergever MA, Nigris DD, Collins DL, Arbel T, Peroni M, Li R, Sharp GC, Schmidt-Richberg A, Ehrhardt J, Werner R, Smeets D, Loeckx D, Song G, Tustison N, Avants B, Gee JC, Staring M, Klien S, Stoel BC, Urschler M, Werlberger M, Vandemeulebroucke J, Rit S, Sarrut D, Pluim PW (2011) Evaluation of registration methods on thoracic CT: the Empire 10 challenge. IEEE Trans Med Imaging 30(11):1901–1920
37. Min Y, Santhanam AP, Neelakkantan H, Ruddy BH, Meeks SL, Kupelian P (2010) A GPU-based framework for modeling real-time 3D lung tumor conformal dosimetry with subject specific lung tumor motion. Phys Med Biol 55(17):5137–5150
38. Santhanam AP, Min Y, Mudur SP, Rastogi A, Ruddy BH, Shah A, Divo E, Kassab A, Rolland JP, Kupelian P (2010) An inverse hyperspherical harmonics based formulation for reconstructing 3D volumetric lung deformations. CR MECANIQUE 338(7–8):461–473